molecules

MDPI

Article

One-Pot Preparation of Layered Double Hydroxide-Engineered Boric Acid Root and Application in Wastewater

Fengrong Zhang [1,*], Cuilan Zhang [2], Kaixuan Zhang [1], Lishun Wu [1] and Dandan Han [1]

[1] School of Chemistry and Chemical Engineering, Heze University, Heze 274015, China; 15254096837@163.com (K.Z.); 19105407006@163.com (L.W.); danicahan1125@163.com (D.H.)
[2] Guiyang Road Primary School, Heze 274015, China; 18754041693@163.com
* Correspondence: zfrong1204@163.com

Abstract: Heavy metals and organic pollutants are prevalent in water bodies, causing great damage to the environment and human beings. Hence, it is urgent to develop a kind of adsorbent with good performance. Anion interlacing layered double hydroxides (LDHs) are a promising adsorbent for the sustainable removal of heavy metal ions and dyes from wastewater. Using aluminum chloride, zinc chloride and ammonium pentaborate tetrahydrate ($NH_4B_5O_8 \cdot 4H_2O$, BA) as raw materials, the LDHs complex (BA-LDHs) of $B_5O_8^-$ intercalation was prepared by one-step hydrothermal method. The BA-LDHs samples were characterized by a X-ray powder diffractometer (XRD), scanning electron microscope (SEM), Fourier transform infrared spectrometer (FT-IR) and the Brunauer–Emmett–Teller (BET) method. The results showed that $B_5O_8^-$ was successfully intercalated. Adsorption experimental results suggested that BA-LDHs possess a maximum adsorption capacity of 18.7, 57.5, 70.2, and 3.12 $mg \cdot g^{-1}$ for Cd(II), Cu(II), Cr(VI) and Methylene blue (MB) at C_s = 2 $g \cdot L^{-1}$, respectively. The adsorption experiment conforms to the Langmuir and Freundlich adsorption models, and the kinetic adsorption data are well fitted by the pseudo-second-order adsorption kinetic equation. The as-prepared BA-LDHs have potential application prospects in the removal of heavy metals and dyes in wastewater. More importantly, they also provide a strategy for preparing selective adsorbents.

Keywords: layered double hydroxides; heavy metals; methylene blue; adsorption; solid concentration effect; $NH_4B_5O_8$

check for updates

Citation: Zhang, F.; Zhang, C.; Zhang, K.; Wu, L.; Han, D. One-Pot Preparation of Layered Double Hydroxide-Engineered Boric Acid Root and Application in Wastewater. *Molecules* **2024**, *29*, 3204. https://doi.org/10.3390/molecules29133204

Academic Editor: Giorgio Vilardi

Received: 11 June 2024
Revised: 25 June 2024
Accepted: 3 July 2024
Published: 5 July 2024

Copyright: © 2024 by the authors. Licensee MDPI, Basel, Switzerland. This article is an open access article distributed under the terms and conditions of the Creative Commons Attribution (CC BY) license (https://creativecommons.org/licenses/by/4.0/).

1. Introduction

Heavy-metal and organic pollution is a significant environmental issue that has raised global concern due to its harmful impact on humans and the natural ecosystem [1]. Cd(II) and Cu(II), as two typical cationic heavy metals, are common in wastewater. Cd(II) and its compounds were included in the list of toxic and hazardous water pollutants (the first batch), and were also in the list of group 1 carcinogens. Excess Cd(II) in the human body can damage the kidney and liver and lead to osteoporosis and the softening of bones. Japan has reported a chronic cadmium poisoning phenomenon known as "Ita-ita-sickness" caused by the ingestion of cadmium-contaminated water sources. In a food sample, rice and rice products in Hunan were found to contain excessive levels of cadmium. Though Cu(II) is one of the essential trace minerals in the human body, if the body ingests too much, it may also cause great harm to organisms and even endanger aquatic organisms and human lives by binding with enzymes and proteins [2,3]. Hexavalent chromium Cr(VI), like Cd(II), was also listed in the list of toxic and hazardous water pollutants (the first batch), and also in the list of group 1 carcinogens. Common species of Cr(VI) in wastewater are CrO_4^{2-}, $H_2Cr_2O_7$, $Cr_2O_7^{2-}$, and $HCrO_4^-$, which have more toxicity compared with Cr(III) and can be easily absorbed and stored, thereby considerably harming human health [4–6]. Cr(VI) can cause kidney and liver damage and has carcinogenic effects. Methylene blue (MB), a commonly used dye, was listed as a group 3 carcinogen by the World Health Organization's

International Agency for Research on Cancer. The harmful components of this kind of dye may be absorbed by the skin and diffuse in the human body after long-term contact, affecting the normal metabolic reaction of the human body [7]. Therefore, the removal of heavy metal ions and dyes from wastewater is of great significance.

Generally, the techniques applied in the treatment of heavy metal ions and dye contamination include chemical precipitation, electro-chemical treatment, ion exchange, membrane filtration, catalysis and the adsorption method. Among these, the chemical precipitation method produces large amount of sludge, which may result in the problem of secondary contamination. Electro-chemical treatment expends a lot of electric energy. Furthermore, the ion-exchange and membrane filtration methods cannot be used at a large scale, owing to their high cost. Of note, catalysis plays a crucial role in many chemical processes, in particular for organic wastes that are hardly degradable through a conventional biodegradation process, such as dyes and textile assistants [8]. However, the adsorption method is an efficient and economical means of removing aqueous heavy metals and dyes [9–12] because of its convenient maintenance and low cost [13,14] in mono-pollutant and binary polluted systems. It involves attracting the pollutants to the surface of adsorbents via coordination bonds, π-π interaction, hydrogen bonds and electrostatic attraction.

Nanomaterials, used as adsorbents to remove heavy metal ions and dyes from wastewater, have received significant attention owing to their high specific surface area. As a nanomaterial, hydrotalcites (also known as layered double hydroxides, LDHs) are a class of anionic layered clays whose chemical composition is $[M^{2+}_{1-x}\ M^{3+}_{x}\ (OH)_2]^{x+}[A^{n-}]_{x/n}\cdot mH_2O$, of which M^{2+} is a bivalent metal ion, such as Mg^{2+}, Zn^{2+}, Cu^{2+}, Co^{2+}, and Ni^{2+}; M^{3+} is a trivalent metal ion, such as Al^{3+}, Fe^{3+}, and Cr^{3+}; and A^{n-} is an interlayer anion, such as NO_3^-, CO_3^{2-}, and Cl^- [15]. The cationic structure layer and interlayer exchangeable ions are connected by non-covalent bonds such as static gravity and hydrogen bonds, mainly hydrogen bonds with weak binding force, among which x is generally between 0.2 and 0.8. Interlayer anions and bound water molecules of hydrotalcite can be exchanged or removed without destroying their own layered structures. The special structure of LDHs gives them the controllability of layer cations, controllability of interlayer anions, and thermal stability, and they are also flame retardant. At the same time, LDHs have been studied and applied more and more widely due to their special properties, and the main applications now include adsorbents, catalysts, ion-exchange carriers, pharmaceutical production, cement additives, wastewater treatment and other industries and fields [16–19].

Boron is an electron-deficient element with strong oxyphilic property and has the characteristics of inorganic polymer elements. It exists mainly in the form of borate in nature. In borate, boron atoms form planar triangular (BO_3) units with sp^2 hybridization, or tetrahedral (BO_4) units with sp^3 hybridization, which can be linked to form mononuclear- or multinuclear-containing boron and oxygen anions. Borates are listed as critical materials, main sources of boron, and have a wide range of industrial applications [20]. Wang et al. reported a study on the effective removal of Cr(VI) by highly crystalline aluminum borate BAC(10), which was hydrothermally synthesized from a mixture of boric acid, anhydrous aluminum trichloride, and ammonium hydroxide at 150 °C for 18 h [21]. However, ammonium hydroxide has the characteristics of volatility and corrosion, and it is limited in the process of use. Most of the LDHs of boric acid intercalation were prepared by the ion-exchange method [22].

This study aims to prepare a new adsorbent through a simple method to improve the adsorption efficiency of $NH_4B_5O_8$-modified LDHs for pollutants. Of late, the preparation of LDHs from $NH_4B_5O_8$ has rarely been reported. Herein, a composite adsorbent (BA-LDHs) was developed using a facile and convenient one-pot synthesis method and then adopted for Cd(II), Cu(II), Cr(VI) and MB adsorption. By characterizing the BA-LDHs and comparing the adsorption performance for different pollutants containing heavy-metal cations (Cd(II), Cu(II)) and anions (Cr(VI)) and dyes (MB), the investigation included the following steps: (1) prepare and characterize BA-LDHs; (2) investigate the removal behaviors of Cd(II), Cu(II), Cr(VI) and MB by this new sorbent; and (3) clarify the mechanisms involved

in Cd(II), Cu(II), Cr(VI) and MB adsorption. BA-LDHs are an economical and practicable material for removing heavy metals and dyes from water and provide a reference for sewage treatment.

2. Results and Discussion

2.1. Characterization of Adsorbents

Figure 1 shows the powder X-ray diffraction (XRD) patterns of all samples in the 2θ range of 5–70°. It is well known that the XRD peak intensity depends on the number of diffraction planes of the incident X-ray quantum at the same 2θ values. The interlayer spacing of the LDH layers was calculated according to Bragg's equation. Observing the XRD spectra of BA-LDH, the primary characteristic peaks corresponded to 2θ~9.99°, 20.1°, 33.9°, 60.3° and 61.2°, namely 003, 006, 009, 110 and 113, respectively, which was closely associated with the lamellar structure of LDH. This observation implies the successful preparation of ZnAl-LDH, which was consistent with the crystal ZnAl-LDHs reported in the literature [23–25]. The corresponding interlayer spacing values at 003, 006 and 009 are 0.89 nm, 0.44 nm and 0.26 nm, respectively. As can be seen, the intensity of the characteristic diffraction peaks of BA decreases in the BA-LDHs, which means that BA was involved in the reaction. The size of $B_5O_8^-$ was calculated by Gauss as 0.86 nm × 0.59 nm × 0.18 nm, which means the pentaborate ions ($B_5O_8^-$) may enter the LDHs interlayer. Except for the increase in peak intensity, no other characteristic peaks were detected in BA-LDHs-Cd, BA-LDHs-Cu, BA-LDHs Cr and BA-LDHs-MB. So, the material consisted of these two phases. This indicates that the adsorbed samples retained their original crystal structures very well.

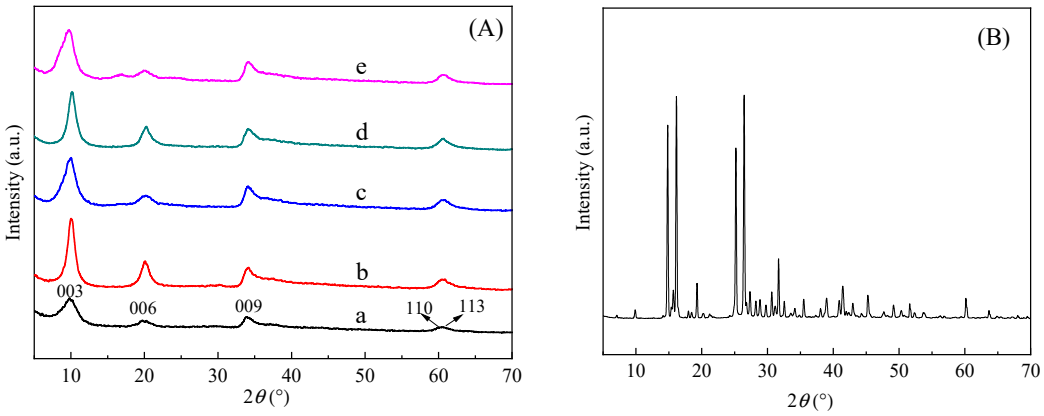


Figure 1. Experimental XRD patterns of (**A**): (a) BA-LDHs, (b) BA-LDHs-Cd, (c) BA-LDHs-Cu, (d) BA-LDHs-Cr and (e) BA-LDHs-MB; (**B**): BA.

The SEM image of $NH_4B_5O_8 \cdot 4H_2O$ (Figure 2a) presents the morphology of a rhombic system with two vertebrae. When $NH_4B_5O_8 \cdot 4H_2O$ was heated above 90 °C, it decomposed and released ammonia, which provided an alkaline environment when preparing BA-LDHs, without adding additional alkaline substances. This method of preparing BA-LDHs was similar to urea hydrolysis, which has rarely been reported. Before adsorption, BA-LDHs' appearance was composed of many small flakes piled up (Figure 2b). However, after the adsorption of Cd(II), Cu(II), Cr(VI) and MB, the morphology of samples changed significantly. The BA-LDHs-Cd and BA-LDHs-Cu showed that the pieces were connected to each other, with loose porous and folded states (Figure 2c,d). The morphology of BA-LDHs-Cr and BA-LDHs-MB had some large sheet structures (Figure 2e,f). The above results were consistent with those of XRD characterization (Figure 1). In the element distribution mapping of the adsorbed samples, it can be seen that Cd(II), Cu(II), Cr(VI) and S (the S element was the MB containing a detection marker) are detected, respectively. Moreover, the surface area of the BA-LDHs was 101.31 $m^2 \cdot g^{-1}$. This was agreed with the reported ZnAl-LDH-BC_{600} (102.56 $m^2 \cdot g^{-1}$), which was from the ZnAl-LDHs modified by biochar

at 600 °C [26]. The pore size (D_p) and pore volume (V_p) of BA-LDHs were 6.67 nm and 0.152 $cm^3 \cdot g^{-1}$, respectively. This demonstrated that the above structure of BA-LDHs could provide a good adsorption site.

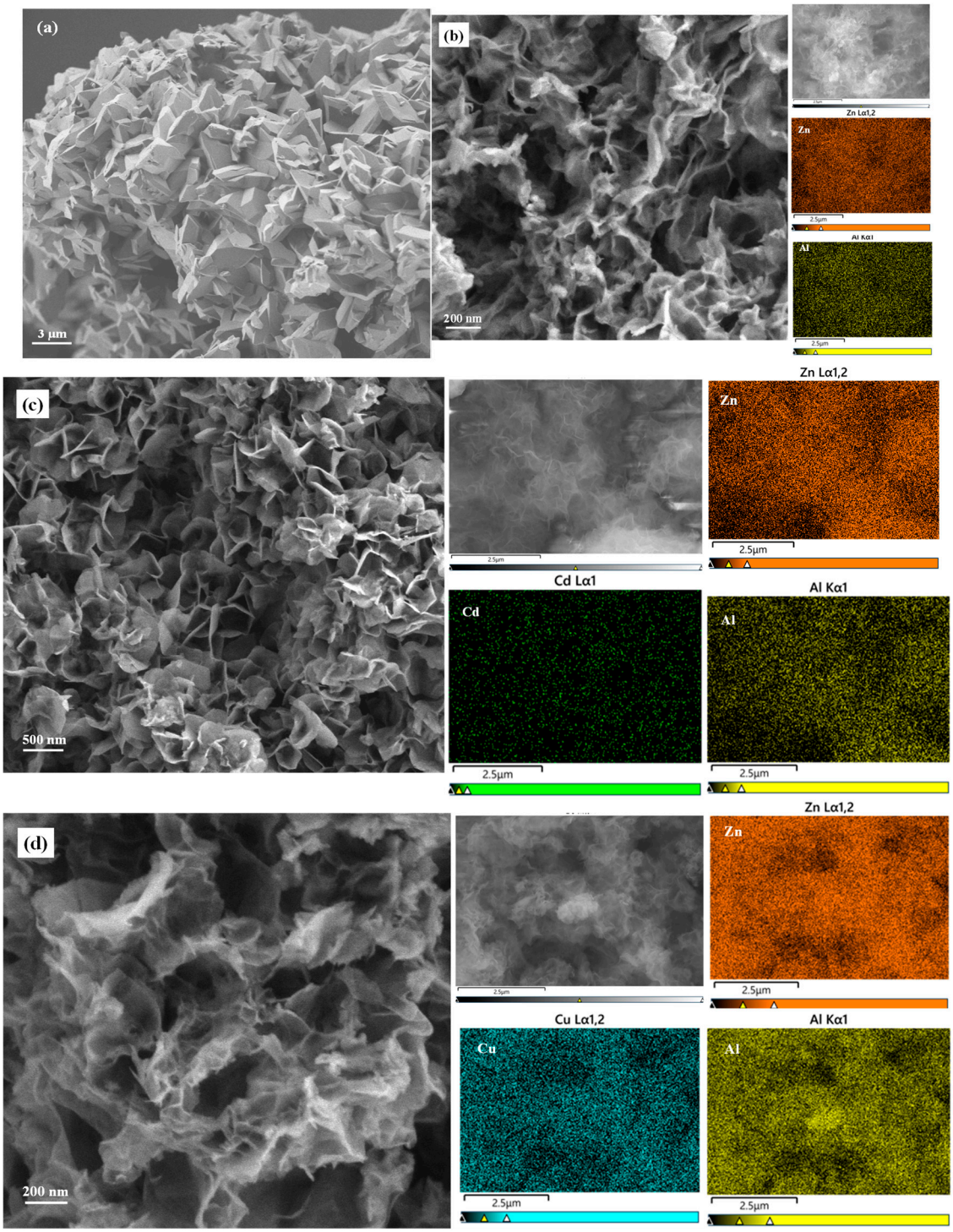


Figure 2. *Cont.*

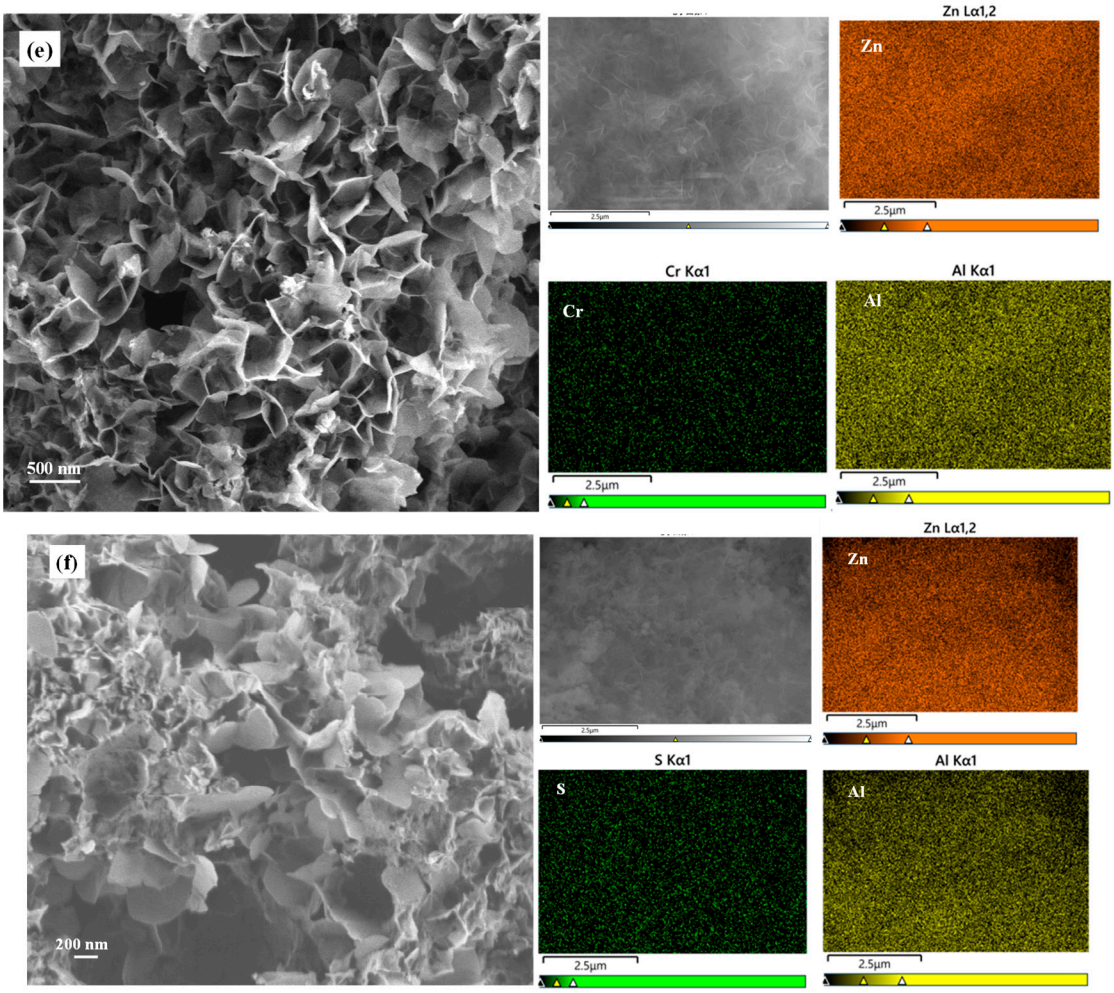


Figure 2. SEM images and corresponding elements distribution mapping of. (**a**) $NH_4B_5O_8 \cdot 4H_2O$; (**b**) BA-LDHs; (**c**) BA-LDHs-Cd; (**d**) BA-LDHs-Cu; (**e**) BA-LDHs-Cr; (**f**) BA-LDHs-MB.

The FT-IR spectra for BA-LDHs, BA-LDHs-Cd, BA-LDHs-Cu, BA-LDHs-Cr and BA-LDHs-MB are presented in Figure 3. There is an intense band around 3470 cm^{-1} in all samples, which corresponds to the stretching of the hydroxyl bond (O-H), relative to both the hydration water of the interlayer space and the hydroxyl group present in the LDH layers [23]. The band at 1340 cm^{-1} was assigned to the stretching of CO_3^{2-} in the samples, which was due to dissolved CO_2 in the aqueous medium [27]. The stretching vibration of the B-O group manifested as a shoulder peak at 1434 cm^{-1} [23]. Additionally, the vibration signals at 1013, 926, 705 and 598 cm^{-1} could be attributed to M–O (Zn-O and Al-O) [23]. Moreover, the vibrational signals at 598 cm^{-1} in BA-LDHs and the phenomenon of redshift, which occurred in all samples after adsorption, indicated that the adsorption mechanism was not consistent in each adsorption system (see Section 3.4. Adsorption mechanism).

2.2. Adsorption Kinetics

The adsorption amount and adsorption speed of the adsorbents on the pollutants could be deduced by kinetic behavior, so as to determine the underlying mechanism. The adsorption kinetics of BA-LDHs to Cd(II), Cu(II), Cr(VI) and MB are shown in Figure 4a. As can be seen from the adsorption kinetics curves of BA-LDHs for Cd(II) and MB, the adsorption equilibrium could be quickly reached within 30 min. However, the adsorption of BA-LDHs for Cu(II) and Cr(VI) comprised two phases of fast adsorption and slow adsorption. At the beginning of the 100 min, the adsorption capacity increased sharply with the increase in adsorption time and then gradually slowed down and reached saturation.

The reason for this phenomenon could be attributed to an abundance of unoccupied active sites on the BA-LDHs at the beginning of the reaction [28], whereas as the reaction continued, the majority of the sites on BA-LDHs were occupied by Cu(II) and Cr(VI), until they were filled [29].

(Cd(II): C_0 = 200 mg·L^{-1}, Cu(II): C_0 = 100 mg·L^{-1}, Cr(VI): C_0 = 100 mg·L^{-1},

MB: C_0 = 4 mg·L^{-1}, 25 °C, C_s = 4 g·L^{-1})

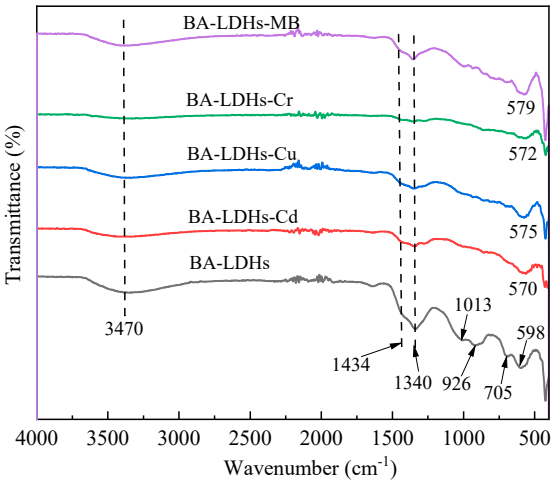


Figure 3. Fourier transform infrared spectroscopy (FT-IR) spectra of samples before and after Cd(II), Cu(II), Cr(VI) and MB adsorption.

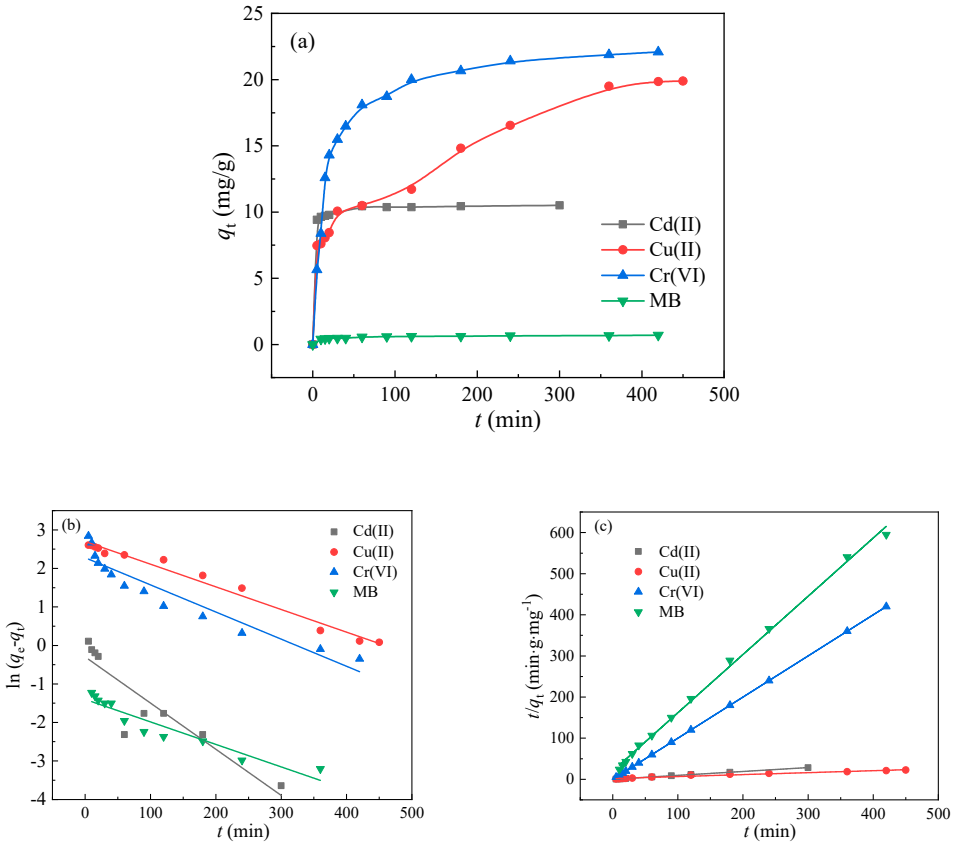


Figure 4. (**a**) Kinetics, (**b**) pseudo-first-order kinetics and (**c**) pseudo-second-order kinetics for Cd(II), Cu(II), Cr(VI) and MB sorption on BA-LDHs samples.

For a better elucidation of the adsorption mechanism, quasi-first-order and quasi-second-order rate equations were used to fit the experimental data, respectively (Figure 4b,c). Table 1 lists the fitted rate equation parameters and linear correlation coefficient (R^2) values. By comparison, the quasi-second-order rate equation can better describe the experimental results.

Table 1. Kinetic model parameters for Cd(II), Cu(II), Cr(VI) and MB adsorption onto BA-LDHs samples (C_s = 4 g·L^{-1}).

Adsorption Object	Pseudo-First-Order: $\ln(q_e - q_t) = \ln q_e - k_1 t$			Pseudo-Second-Order: $t/q_t = 1/q_e^2 k_2 + t/q_e$		
	q_e	k_1	R^2	q_e	k_2	R^2
Cd	0.7421	0.01199	0.8003	10.54	0.08180	0.9999
Cu	14.85	0.005880	0.9794	20.98	0.001189	0.9736
Cr	9.746	0.007050	0.8955	22.79	0.002853	0.9997
MB	0.2463	0.005840	0.8946	0.7063	0.09844	0.9974

2.3. Adsorption Isotherms

An adsorption isotherm is an important tool to obtain the information about the properties of adsorption layers and the interaction between adsorbed and adsorbed substances [30]. Langmuir and Freundlich, as broadly accepted isotherm models, were introduced in the present study to elaborate the adsorption behavior of Cd(II), Cu(II), Cr(VI) and MB onto BA-LDHs. The Langmuir model is based on the premise that monolayer adsorption occurs on a uniform surface, and it could be used to predict the maximum adsorption capacity of the adsorbent [31]. According to the Freundlich model, the surface of the adsorbent is heterogeneous, and the adsorbent is adsorbed in multiple layers [32]. The Langmuir and Freundlich isotherms were used for the nonlinear fitting of the above adsorption equilibrium data, respectively. The results showed that both Langmuir and Freundlich isotherms could describe the adsorption isotherms of the adsorption system under each C_s (Figure 5). Table 2 lists the fitting values of the model parameters by Langmuir and Freundlich isothermal equations. It could be seen that the saturation adsorption q_m decreases with the increase in C_s, which was known as the solid concentration effect [33–35]. It was found that other parameters also change with the change of C_s. However, neither the Langmuir nor Freundlich isotherm could describe or predict this phenomenon.

Table 2. Nonlinear-fit data of model parameters for Cd(II), Cu(II), Cr(VI) and MB sorption on BA-LDHs at different C_s.

Adsorption Object	C_s (g·L^{-1})	Langmuir Isotherm: $q_e = K_L q_m C_e/(1 + q_m K_L)$			Freundlich Isotherm: $q_e = K_F C_e^{n_F}$		
		q_m (mg·g^{-1})	K_L (L·mg^{-1})	R^2	n_F	K_F (mg$^{1-n_F}$L^{nF}·g^{-1})	R^2
Cd	2	18.7	0.004	0.952	0.608	0.303	0.904
	4	10.9	0.006	0.925	0.601	0.228	0.877
	8	5.65	0.007	0.952	0.565	0.148	0.911
Cu	2	57.5	0.0458	0.965	0.330	9.40	0.996
	4	50.1	0.0338	0.971	0.362	6.74	0.999
	8	38.6	0.0642	0.977	0.359	6.05	0.976
Cr	2	70.2	0.0347	0.997	0.358	9.57	0.954
	4	52.3	0.0273	0.982	0.489	3.85	0.948
	8	32.2	0.0179	0.991	0.531	1.71	0.987
MB	2	3.12	0.0285	0.989	0.408	0.351	0.986
	4	1.58	0.0332	0.978	0.522	0.121	0.940
	8	0.930	0.0387	0.930	0.618	0.0524	0.927

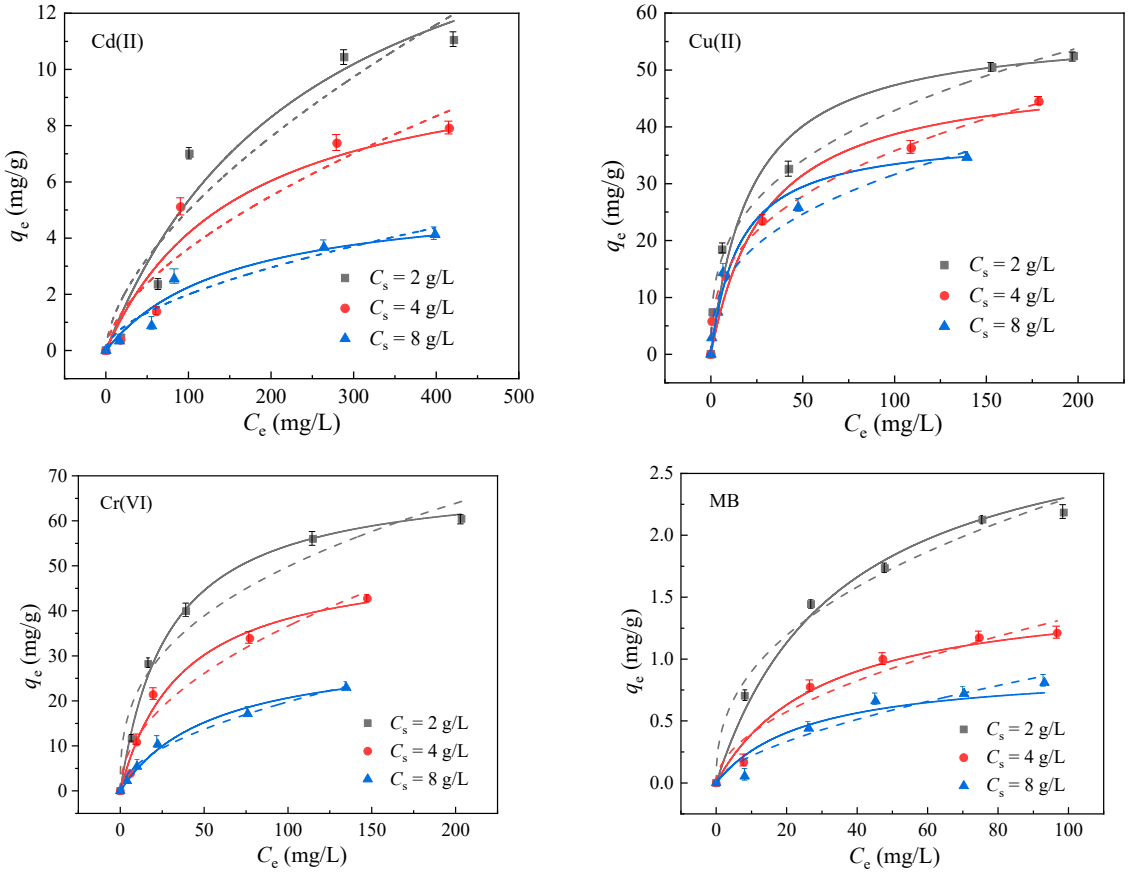


Figure 5. Sorption isotherms of Cd(II), Cu(II), Cr(VI) and MB adsorption onto BA-LDHs at different sorbent dosages. (25 °C). The dots represent experimental data, the solid lines represent Langmuir model fits, and the dashed lines represent Freundlich model fits.

2.4. Adsorption Mechanism

Overall, taking into account the characterization analysis and batch adsorption experimental results, the adsorptions of Cd(II), Cu(II), Cr(VI) and MB on BA-LDHs were complex process concerning several specific mechanisms. The apparently optimized porosity structure and expanded surface area (BET and SEM) of BA-LDHs yielded an abundance of available sorption sites for Cd(II), Cu(II), Cr(VI) and MB to be filled in the pores channel. The Freundlich isotherm model matched experimental data well, illustrating that the surface sites of BA-LDHs were heterogeneous, and its entrapment of Cd(II), Cu(II), Cr(VI) and MB could be driven by multilayer physical adsorption. According to the saturated adsorption capacity (q_m) of BA-LDHs for pollutants, the adsorption capacity for each pollutant is Cr(VI) > Cu(II) > Cd(II) > MB at C_s = 2 g·L^{-1} (Table 2). Briefly, the main mechanism of Cr(VI) removal from water was tied to the isomorphic substitution of Cr^{6+} and Zn^{2+} and the intercalation of $Cr_2O_7^{2-}$, except $Cr(OH)_3$ precipitation. The former is because the radius of Cr^{6+} (0.044 nm) is smaller than the radius of Zn^{2+} (0.074 nm), and the latter is because the successful intercalation of $B_5O_8^-$ (0.86 nm × 0.59 nm × 0.18 nm) in the early stage opens a channel for $Cr_2O_7^{2-}$ (0.55 nm × 0.25 nm × 0.21 nm) to enter. The main mechanism of removal of Cu(II) from water is isomorphic substitution, except $Cu(OH)_2$ precipitation, mainly because the ionic radius of Cu(II) (0.073 nm) is very close to that of Zn^{2+} (0.074 nm). The main mechanism of Cd(II) removal from water is $Cd(OH)_2$ precipitation on the surface of the adsorbent. The main mechanism of MB removal was on account of H-bonding and complexation. A suggested reaction pathway for the adsorption is presented in Figure 6.

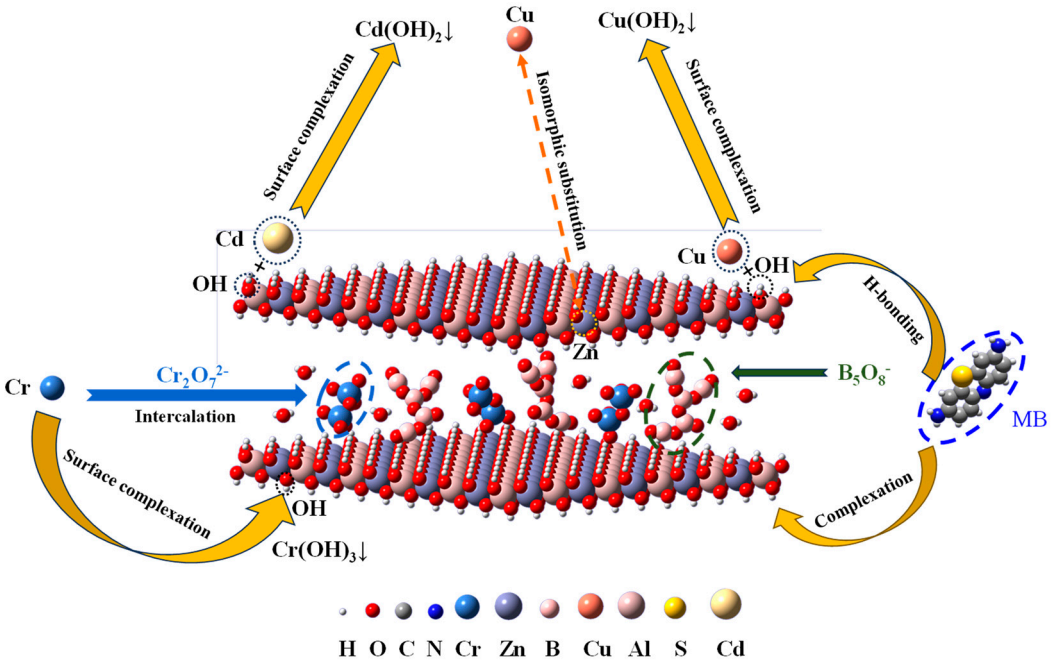


Figure 6. Proposed mechanism schematic.

3. Materials and Methods

3.1. Chemicals and Materials

The reagents required for the current work were of analytical grade. Aluminum chloride hexahydrate ($AlCl_3 \cdot 6H_2O$), zinc chloride ($ZnCl_2$) and cadmium pellets were purchased from Tianjin Kemi Ou Chemical Reagent Co., Ltd., Tianjin, China. Nitric acid (HNO_3), cupric nitrate ($Cu(NO_3)_2$) and potassium dichromate ($K_2Cr_2O_7$) were purchased from Sinopharm Chemical Reagent Co., Ltd., Shanghai, China. Urea was purchased from Shanghai Aladdin Biochemical Technology Co., Ltd., Shanghai, China. Pentaborate amine tetrahydrate ($NH_4B_5O_8 \cdot 4H_2O$) was purchased from Shanghai Maclin Biochemical Technology Co., Ltd., Shanghai, China. Water was purified with a Hitech-Kflow water purification system (Hitech, Beijing, China) (DW).

3.2. Fabrication of BA-LDHs Composites

A composite adsorbent (BA-LDHs) was manufactured by a one-pot hydrolysis method with $ZnCl_2$, $AlCl_3 \cdot 6H_2O$ and boric acid root ($B_5O_8^-$). Specifically, first, 0.4080 g of $ZnCl_2$, 0.2414 g of $AlCl_3 \cdot 6H_2O$ with a Zn/Al molar ratio of 3:1, and 2.720 g of $NH_4B_5O_8 \cdot 4H_2O$ (BA) were mixed by a digital-display constant-temperature magnetic stirrer (XMTD-204, Jintan city Jiangnan Instrument Factory, Jinan, China) thoroughly in 60 mL aqueous solution for 30 min to obtain a homogeneous suspension. Next, the aqueous dispersion obtained above was transferred to in a 100 mL Teflon-lined stainless-steel reactor for 24 h at 120 °C. The reaction solution was centrifuged at 7500 rpm using a centrifuge (TG16-WS, Changsha Xiangzhi centrifuge Instrument Co., Ltd., Changsha, China). The obtained sediment was washed with DW repeatedly until the pH of the solution remained near 7. Then, the obtained samples were dried at 70 °C for 12 h in an electric thermostatic oven (DHG-9070A, Shanghai Haozhuang Instrument Co., Ltd., Shanghai, China). Finally, the product obtained after grinding using an agate mortar was denoted as BA-LDHs.

3.3. Characteristics of Adsorbents

The crystalline mineral ingredients of BA-LDHs and samples after adsorption were determined by powder X-ray diffraction (XRD, D/max-rA, Bruker AXS, Co., Ltd., Karlsruhe, Germany) at 40 kV and 40 mA in the 2θ range of 1–10° at a scanning rate of 1°/min and 10–70° at a scanning rate of 10°/min, respectively. The analysis area was more than

2 mm × 2 mm. The morphologies of BA-LDHs and LDHs samples were analyzed using GeminiSEM 300 scanning electron microscopy (Carl Zeiss (Shanghai) Management Co., Ltd., Oberkochen, Germany) under the conditions of 1 kV acceleration voltage, coated with gold-palladium. The specific surface area (A_s) and pore volume (V_p) of the samples were calculated using the Brunauer–Emmett–Teller (BET) and Barrett–Joyner–Halenda (BJH) methods, respectively. The surface functional groups of BA-LDHs and samples after adsorption were determined via a Fourier transform infrared spectrum (FTIR, Nicolet 5700, Thermo, Waltham, MA, USA) in the range of 500–3900 cm^{-1} with a resolution of 4 cm^{-1}, and scanning was performed in parallel 256 times.

3.4. Adsorption Experiments

The adsorption behavior and mechanisms of the adsorbents with the best sorption capacity for Cd(II), Cu(II), Cr(VI) and MB were then investigated through adsorption kinetics and isotherms.

The Cd(II), Cu(II), Cr(VI) and MB removal tests were carried out at room temperature. The initial concentrations of Cd(II) from 20 to 450 $mg{\cdot}L^{-1}$ were prepared by dissolving cadmium pellets in nitric acid and deionized water; initial concentrations of Cu(II) from 10 to 280 $mg{\cdot}L^{-1}$ were prepared by dissolving $Cu(NO_3)_2$ in deionized water; initial concentrations of Cr(VI) from 20 to 300 $mg{\cdot}L^{-1}$ were prepared by dissolving $K_2Cr_2O_7$ in deionized water; and initial concentrations of MB from 3.5 to 70 $mg{\cdot}L^{-1}$ were prepared by dissolving methylene blue in deionized water. In all the above solutions, 0.010 M of $NaNO_3$ was applied as maintainer for the constant ionic strength of the solutions. With the usage of 0.1 M HNO_3 and NaOH solutions, the pH values of the Cd(II), Cu(II), Cr(VI) and MB solutions were adjusted to 5.5.

Adsorption kinetics provided important guidance to estimate the possible adsorption mechanisms. Briefly, the BA-LDHs was accurately weighed (C_s = 4 $g{\cdot}L^{-1}$) in different beakers containing Cd(II): C_0 = 200 $mg{\cdot}L^{-1}$, Cu(II): C_0 = 100 $mg{\cdot}L^{-1}$, Cr(VI): C_0 = 100 $mg{\cdot}L^{-1}$, and MB: C_0 = 4 $mg{\cdot}L^{-1}$ solutions, respectively. Then, the solution was oscillated at 150 r/min at room temperature and sampled at different times (0–450 min). Then, we took an appropriate amount of the solution through a 0.45 μm filter membrane and tested the concentration of Cd(II) and Cu(II) in the filtrate using an atomic absorption spectrophotometer (AAS) (AAS-3600, Shanghai Metash Instruments Co., Ltd., Shanghai, China) equipped with an air-acetylene flame, and Cr(VI) and MB using a visible spectrophotometer (N-5600PC, Shanghai Yuan Analysis Instrument Co., Ltd., Shanghai, China). The experimental error was determined by conducting parallel experiments. Information about the kinetic models, including the pseudo-first-order kinetic model and pseudo-second-order kinetic model, was used to fit the experimental data (see Figure 4 and Table 1).

The adsorption isotherm model could provide important guidance for the adsorption of heavy metals and dyes in solution. Briefly, a certain amount of BA-LDHs was weighed and put into a polyethylene tube containing a certain volume of the above solution: Cd(II) from 20 to 450 $mg{\cdot}L^{-1}$; Cu(II) from 10 to 280 $mg{\cdot}L^{-1}$; Cr(VI) from 20 to 300 $mg{\cdot}L^{-1}$; and MB from 3.5 to 70 $mg{\cdot}L^{-1}$. The adsorbent dosages were kept at 2 $g{\cdot}L^{-1}$, 4 $g{\cdot}L^{-1}$ and 8 $g{\cdot}L^{-1}$ in different solutions. Then, the above solutions were oscillated at 150 r/min on a thermostatic oscillator until adsorption reached equilibrium. Langmuir and Freundlich isotherm models were introduced to elaborate the adsorption behavior of Cd(II), Cu(II), Cr(VI) and MB onto BA-LDHs (see Figure 5 and Table 2).

Moreover, all tests in the present work were executed in triplicate, and the relative error was less than 4.8%.

The adsorption capacity (q_t or q_e ($mg{\cdot}g^{-1}$)) of adsorbents for the target pollutants (Cd(II), Cu(II), Cr(VI) and MB) was computed according to the following Formulas (1) and (2).

$$q_t = (C_0 - C_t)/C_s \quad (1)$$

$$q_e = (C_0 - C_e)/C_s \quad (2)$$

The C_0, C_t, C_s, and C_e parameters denote initial concentration, concentration of the solution at time *t*, adsorbent dosage, and the concentration of solution at the adsorption equilibrium, respectively.

The samples after Cu(II),Cd(II), Cr(VI) and MB adsorption by BA-LDHs were denoted as BA-LDHs-Cu, BA-LDHs-Cd, BA-LDHs-Cr and BA-LDHs-MB, respectively.

4. Conclusions

A BA-LDH composite was manufactured by a facile one-pot pyrolysis approach with $ZnCl_2$, $AlCl_3 \cdot 6H_2O$ and boric acid root ($B_5O_8^-$). The BA-LDH samples were characterized by XRD, SEM, FT-IR and BET. The results showed that borate was successfully intercalated. And it exhibited Cd(II), Cu(II), Cr(VI) and MB adsorption ability. Adsorption experimental results suggested that BA-LDHs possess a maximum adsorption capacity of 18.7, 57.5, 70.2, and 3.12 $mg \cdot g^{-1}$ for Cd(II), Cu(II), Cr(VI) and MB at C_s = 2 $g \cdot L^{-1}$, respectively. The kinetic adsorption data were well fitted by the pseudo-second-order adsorption kinetic equation. The adsorption isotherms conformed to the Langmuir and Freundlich adsorption models. The main mechanism of Cd(II), Cr(VI) and MB removal from water were tied to isomorphic substitution and the intercalation of $Cr_2O_7^{2-}$, except $Cr(OH)_3$ precipitation; Cu(II) was owing to isomorphic substitution, except $Cu(OH)_2$ precipitation; Cd(II) removal was due to $Cd(OH)_2$ precipitation on the surface of the adsorbent; and MB removal was due to H-bonding and complexation. The as-prepared BA-LDHs have potential application prospects in the removal of heavy metals and dyes in wastewater. More importantly, this also provides a strategy for preparing selective adsorbents.

Author Contributions: F.Z. conceived and designed the experiment. She performed the experiments and carried out the data analysis. C.Z. and L.W. polished the grammar of the manuscript. D.H. and K.Z. carried out characterization experiments on the samples. All authors have read and agreed to the published version of the manuscript.

Funding: This work is supported financially by the project of Shandong Province higher educational science and technology program (No. J18KA104), Hubei Province central government guide local science and technology development project (No. 2204-429006-04-02-813827) and the horizontal research project of process optimization of febuxostat API for Hubei Huashitong (No. 010008002040030).

Institutional Review Board Statement: Not applicable.

Informed Consent Statement: Not applicable.

Data Availability Statement: The data supporting the findings of this study are available within the article.

Conflicts of Interest: The authors declare that they have no known competing financial interests or personal relationships that could have appeared to influence the work reported in this paper.

References

1. Kurwadkar, S. Occurrence and distribution of organic and inorganic pollutants in groundwater. *Water Environ. Res.* **2019**, *91*, 1001–1008. [CrossRef]
2. Zeng, X.; Zhu, J.; Zhang, G.; Wu, Z.; Lu, J.; Ji, H. Molecular-level understanding on complexation-adsorption-degradation during the simultaneous removal of aqueous binary pollutants by magnetic composite aerogels. *Chem. Eng. J.* **2023**, *468*, 143536. [CrossRef]
3. Wang, Q.Y.; Li, L.P.; Kong, L.C.; Cai, G.Y.; Wang, P.; Zhang, J.; Zuo, W.; Tian, Y. Compressible amino-modified carboxymethyl chitosan aerogel for efficient Cu(II) adsorption from wastewater. *Sep. Purif. Technol.* **2022**, *293*, 121146. [CrossRef]
4. Chen, B.; Yue, W.L.; Zhao, H.N.; Long, F.X.; Cao, Y.R.; Pan, X.J. Simultaneous capture of methyl orange and chromium(VI) from complex wastewater using polyethylenimine cation decorated magnetic carbon nanotubes as a recyclable adsorbent. *ACS Adv.* **2019**, *9*, 4722. [CrossRef]
5. Wang, Y.; Yu, L.; Wang, R.; Wang, Y.; Zhang, X. A novel cellulose hydrogel coating with nanoscale Fe(0) for Cr(VI) adsorption and reduction. *Sci. Total. Environ.* **2020**, *726*, 138625. [CrossRef]
6. Li, Y.F.; Wen, J.; Xue, Z.Z.; Yin, X.Y.; Yuan, L.; Yang, C.L. Removal of Cr(VI) by polyaniline embedded polyvinyl alcohol/sodium alginate beads–Extension from water treatment to soil remediation. *J. Hazard. Mater.* **2021**, *426*, 127809. [CrossRef]

7. Zeng, X.C.; Zhang, G.H.; Wen, J.; Li, X.L.; Zhu, J.F.; Wu, Z. Simultaneous removal of aqueous same ionic type heavy metals and dyes by a magnetic chitosan/polyethyleneimine embedded hydrophobic sodium alginate composite: Performance, interaction and mechanism. *Chemosphere* **2023**, *318*, 137869. [CrossRef]
8. Yang, L.; Jiao, Y.; Xu, X.; Pan, Y.; Su, C.; Duan, X.; Sun, H.; Liu, S.; Wang, S.; Shao, Z. Superstructures with atomic-level arranged perovskite and oxide layers for advanced oxidation with an enhanced non-free radical pathway. *ACS Sustain. Chem. Eng.* **2022**, *10*, 1899–1909. [CrossRef]
9. Guo, L.; Zhang, Y.; Zheng, J.; Shang, L.; Shi, Y.; Wu, Q.; Liu, X.; Wang, Y.; Shi, L.; Shao, Q. Synthesis and characterization of ZnNiCr-layered double hydroxides with high adsorption activities for Cr(VI). *Adv. Compos. Hybrid Mater.* **2021**, *4*, 819–829. [CrossRef]
10. Tang, J.; Ma, Y.; Deng, Z.; Li, P.; Qi, X.; Zhang, Z. One-pot preparation of layered double oxides-engineered biochar for the sustained removal of tetracycline in water. *Bio. Technol.* **2023**, *381*, 129119. [CrossRef]
11. Liang, W.; Wang, G.; Peng, C.; Tan, J.; Wan, J.; Sun, P.; Li, Q.; Ji, X.; Zhang, Q.; Wu, Y.; et al. Recent advances of carbon-based nano zero valent iron for heavy metals remediation in soil and water: A critical review. *J. Hazard Mater.* **2022**, *426*, 127993. [CrossRef]
12. Liang, X.; Su, Y.; Wang, X.; Liang, C.; Tang, C.; Wei, J.; Liu, K.; Ma, J.; Yu, F.; Li, Y. Insights into the heavy metal adsorption and immobilization mechanisms of CaFe-layered double hydroxide corn straw biochar: Synthesis and application in a combined heavy metal-contaminated environment. *Chemosphere* **2023**, *313*, 137467. [CrossRef]
13. Chai, W.S.; Cheun, J.Y.; Kumar, P.S.; Mubashir, M.; Majeed, Z.; Banat, F.; Ho, S.H.; Show, P.L. A review on conventional and novel materials towards heavy metal adsorption in wastewater treatment application. *J. Clean. Prod.* **2021**, *296*, 126589. [CrossRef]
14. Feng, Z.; Zheng, Y.; Wang, H.; Feng, C.; Chen, N.; Wang, S. Sodium humate based double network hydrogel for Cu and Pb removal. *Chemosphere* **2023**, *313*, 137558. [CrossRef]
15. Zubair, M.; Ihsanullah, I.; Aziz, H.A.; Ahmad, M.A.; Al-Harthi, M.A. Sustainable wastewater treatment by biochar/layered double hydroxide composites: Progress, challenges, and outlook. *Bio. Technol.* **2021**, *319*, 124128. [CrossRef]
16. Millange, F.; Walton, R.I.; Lei, L.; O'Hare, D. Efficient separation of terephthalate and phthalate anions by selective ion-Exchange intercalation in the layered double hydroxide $Ca_2Al(OH)_6{\cdot}NO_3{\cdot}2H_2O$. *Chem. Mater.* **2000**, *12*, 1990–1994. [CrossRef]
17. Alcântara, A.C.S.; Aranda, P.; Darder, M.; Ruiz-Hitzky, E. Bionanocomposites based on alginate-zein/layered double hydroxide materials as drug delivery systems. *J. Mater. Chem.* **2010**, *20*, 9495–9504. [CrossRef]
18. Raki, L.; Beaudoin, J.; Alizadeh, R.; Makar, J.; Sato, T. Cement and concrete nanoscience and nanotechnology. *Materials* **2010**, *3*, 918–942. [CrossRef]
19. Basu, D.; Das, A.; George, J.; Wang, D.; Stöckelhuber, K.; Wagenknecht, U.; Leuteritz, A.; Kutlu, B.; Reuter, U.; Heinrich, G. Unmodified LDH as reinforcing filler for XNBR and the development of flame-retardant elastomer composites. *Rubber Chem. Technol.* **2014**, *87*, 606–616. [CrossRef]
20. Peng, Z.-K.; Peng, Q.-M.; Ma, Y.-Q. Thermal characteristics of borates and its indication for endogenous borate deposits. *Ore Geol. Rev.* **2022**, *145*, 104887. [CrossRef]
21. Wang, S.; Bai, P.; Cichocka, M.O.; Cho, J.; Willhammar, T.; Wang, Y.; Yan, W.; Zou, X.; Yu, J. Two-Dimensional cationic aluminoborate as a new paradigm for highly selective and efficient Cr(VI) capture from aqueous solution. *JACS Au* **2022**, *2*, 1669–1678. [CrossRef]
22. Nyambo, C.; Wilkie, C.A. Layered double hydroxides intercalated with borate anions: Fire and thermal properties in ethylene vinyl acetate copolymer. *Polym. Degrad. Stabil.* **2009**, *94*, 506–512. [CrossRef]
23. Zheng, J.; Fan, C.; Li, X.; Yang, Q.; Wang, D.; Duan, A.; Pan, S. Tourmaline/ZnAL-LDH nanocomposite based photocatalytic system for efficient degradation of mixed pollutant wastewater. *Sep. Purif. Technol.* **2024**, *345*, 127306. [CrossRef]
24. Ba, W.; Tang, Y.; Yu, J.; Ya, W.; Wang, C.; Li, Y.; Wang, Z.; Yang, J.; Zhang, L.; Yu, F. Si-doped ZnAl-LDH nanosheets by layer-engineering for efficient photoelectrocatalytic water splitting, Appl. *Catal. B Environ. Energy* **2024**, *346*, 123706. [CrossRef]
25. Sun, S.; Zhang, Y.; Gao, Q.; Zhang, N.; Hu, P.; Feng, W. ZnAl-LDH film for self-powered ultraviolet photodetection. *Nano Mater. Sci.* 2024, *in press*. [CrossRef]
26. Hameed, R.; Abbas, A.; Lou, J.; Khatta, W.; Roh, B.; Iqbal, B.; Li, G.; Zhang, Q.; Zhao, X. Synthesis of biochar-ZnAl-layered double hydroxide composite for effective heavy metal adsorption: Exploring mechanisms and structural transformations. *J. Environ. Chem. Eng.* **2024**, *12*, 112687. [CrossRef]
27. Aquin, R.; Lucen, P.; Arias, S.; Landers, R.; Pacheco, J.A.; Rocha, O. Influence of terephthalate anion in ZnAl layered double hydroxide on lead ion removal: Adsorption, kinetics, thermodynamics and mechanism. *Colloid Surface A* **2024**, *686*, 133404. [CrossRef]
28. Theamwong, N.; Intarabumrung, W.; Sangon, S.; Aintharabunya, S.; Ngernyen, Y.; Hunt, A.J.; Supanchaiyamat, N. Activated carbons from waste Cassia bakeriana seed pods as high-performance adsorbents for toxic anionic dye and ciprofloxacin antibiotic remediation. *Bioresour. Technol.* **2021**, *341*, 125832. [CrossRef]
29. Yao, B.; Luo, Z.; Du, S.; Yang, J.; Zhi, D.; Zhou, Y. Sustainable biochar/$MgFe_2O_4$ adsorbent for levofloxacin removal: Adsorption performances and mechanisms. *Bioresour. Technol.* **2021**, *340*, 125698. [CrossRef]
30. Cheng, D.; Ngo, H.H.; Guo, W.; Chang, S.W.; Nguyen, D.D.; Zhang, X.; Varjani, S.; Liu, Y. Feasibility study on a new pomelo peel derived biochar for tetracycline antibiotics removal in swine wastewater. *Sci. Total Environ.* **2020**, *720*, 137662. [CrossRef]

31. Li, X.; Xu, J.; Shi, J.; Luo, X. Rapid and efficient adsorption of tetracycline from aqueous solution in a wide pH range by using iron and aminoacetic acid sequentially modified hierarchical porous biochar. *Bioresour. Technol.* **2022**, *346*, 126672. [CrossRef] [PubMed]
32. Yan, L.; Liu, Y.; Zhang, Y.; Liu, S.; Wang, C.; Chen, W.; Liu, C.; Chen, Z.; Zhang, Y. $ZnCl_2$ modified biochar derived from aerobic granular sludge for developed microporosity and enhanced adsorption to tetracycline. *Bioresour. Technol.* **2020**, *297*, 122381. [CrossRef] [PubMed]
33. Bakshi, S.; Banik, C.; Rathke, S.J.; Laird, D.A. Arsenic sorption on zero-valent iron-biochar complexes. *Water Res.* **2018**, *137*, 153–163. [CrossRef] [PubMed]
34. Wanga, T.; Lia, C.; Wang, C.; Wang, H. Biochar/MnAl-LDH composites for Cu (II) removal from aqueous solution. *Colloids Surf. A* **2018**, *538*, 443–450. [CrossRef]
35. Nie, Y.; Zhao, C.; Zhou, Z.; Kong, Y.; Ma, J. Hydrochloric acid-modified fungi-microalgae biochar for adsorption of tetracycline hydrochloride: Performance and mechanism. *Bioresour. Technol.* **2023**, *383*, 129224. [CrossRef]

Disclaimer/Publisher's Note: The statements, opinions and data contained in all publications are solely those of the individual author(s) and contributor(s) and not of MDPI and/or the editor(s). MDPI and/or the editor(s) disclaim responsibility for any injury to people or property resulting from any ideas, methods, instructions or products referred to in the content.